

Variability-selected active galactic nuclei from supernova search in the Chandra deep field south

D. Trevese¹, K. Boutsia^{1,2}, F. Vagnetti³, E. Cappellaro⁴, S. Puccetti⁵

¹ Dipartimento di Fisica, Università di Roma “La Sapienza”, P.le A. Moro 2, I-00185 Roma, Italy

² European Southern Observatory, Karl-Schwarzschild-Strasse 2, Garching D-85748, Germany

³ Dipartimento di Fisica, Università di Roma “Tor Vergata”, via delle Ricerca Scientifica, 12, I-00133, Roma, Italy

⁴ INAF - Osservatorio Astronomico di Padova, Vicolo dell’Osservatorio 5, I- 35122 Padova, Italy

⁵ ASI Science Data Centre, c/o ESRIN, via G. Galilei, I00044 Frascati Italy

01 April 2008

ABSTRACT

Context. Variability is a property shared by virtually all active galactic nuclei (AGN), and it was adopted as a criterion to select them using multi epoch surveys. Low Luminosity AGNs (LLAGNs) are contaminated by the light of the host galaxies, thus they cannot be detected by the usual color techniques. For this reason their evolution in cosmic time is poorly known. Consistency with the evolution derived from X-ray detected samples has not been clearly established so far, also because the low luminosity population consists of a mixture of different object types. LLAGNs can be detected through the nuclear optical variability of extended objects.

Aims. Several variability surveys have been, or are being, conducted for the detection of supernovae (SNe). We want to re-analyse SN data with a variability criterion optimised for AGN detection, to select a new AGN sample and study its properties.

Methods. We analysed images taken with the wide field imager at the 2.2 m ESO/MPI telescope, in the framework of the STRESS supernova survey. We selected the AXAF field centred in the Chandra Deep Field South where, besides the deep X-ray survey, various optical data exist, coming from the EIS and COMBO-17 photometric surveys and the spectroscopic database of GOODS.

Results. We obtained a catalog of 132 variable AGN candidates. Several of them are X-ray sources. We compare our results with a recent HST variability study of X-ray and IR detected AGNs, obtaining consistent results. The relatively high fraction of confirmed AGNs in our sample (60%) allowed us to extract a list of reliable AGN candidates for spectroscopic observations.

Key words. Surveys - Galaxies: active - Quasars: general - X-rays: galaxies

1. Introduction

The optical variability of quasars (QSOs) was discovered even before the very nature of their emission lines was understood (Matthews & Sandage 1963). A sharp decline in cosmic time of both radio- and optically-detected QSO populations was established soon after their discovery (Schmidt 1968, 1970). To our knowledge, the use of variability as a tool to detect QSOs was proposed for the first time by van den Berg, Herbst, & Pritchett (1973). In fact any of the QSO properties, like non-stellar color, broad emission lines or variability, can be adopted to select statistically relevant QSO samples. It is just the comparison among samples selected by different techniques which enables to assess the relevant selection effects and to derive the intrinsic cosmological evolution of the QSO population. As the early history of QSO astronomy tells us, the different techniques may also detect related but different classes of objects, as it was the case for the UV excess selection which led to the discovery of radio-quiet QSOs, which are 5-10 times more numerous than the radio-loud ones (e.g. Kellermann et al. 1989; Jiang et al. 2007). The present knowledge of the evolution in cosmic time of the QSO luminosity function (LF) is mainly based on the 2QZ survey (Boyle et al. 2000; Croom et al. 2001) for $z < 2.5$, on spectroscopic surveys for $z \geq 3$ (Warren, Hewett & Osmer 1994; Schmidt, Schneider, & Gunn 1995), and on the Sloan

Digital Sky Survey (SDSS) data for $z > 4.5$ (Fan et al. 2001; Anderson et al. 2001). The above analyses led to a consensus scenario where a fast increase in cosmic time of the QSO number density, down to $z \sim 2$, is followed by a slower decline of the LF, which can be described by luminosity evolution. This is also confirmed by the recent analysis by Richards et al. (2006) which, however, is not the best suited to locate the epoch of maximum number density of active galactic nuclei (AGNs). Both 2QZ and SDSS QSO candidates are selected on the basis of non-stellar colors. This selection technique is limited to point-like objects, namely bright active nuclei overshining the host galaxy which, otherwise, could itself produce non-stellar colors. The most accurate determination of the epoch of maximum density has been obtained by Wolf et al. (2003) based on the COMBO-17 survey, which provides a “low resolution spectrum” allowing to drop the “point-like” condition, to select AGNs on the sole basis of their SED. The analysis of this survey indicates that the epoch of maximum density corresponds to $z \approx 2$ and it is independent of QSO luminosity. But, even in this case, the selection is limited to nuclei brighter than $M_B \approx -21.5$, since otherwise the SED is dominated by the host galaxy light, which prevents recognising the nuclear spectrum. Since van den Berg, Herbst, & Pritchett (1973), variability was adopted as a tool to select QSOs/AGNs in various studies (Usher 1978; Hawkins 1983; Cristiani, Vio & Andreani 1990; Trevese et al. 1989; Véron & Hawkins 1995; Geha et al. 2003). An important aspect of variability as an AGN search technique is that it can be applied to objects with extended images. These

correspond just to low luminosity AGNs (LLAGNs) which cannot be detected by the (non-stellar) color selection since their SED is contaminated (or even dominated) by the light of the host galaxy. In this case, variability selection is also made easier by the fact that the nuclear variability tends to increase for decreasing nuclear luminosity (Hook et al. 1994; Trevese et al. 1994; Cristiani et al. 1996). Bershadsky, Trevese & Kron (1998) selected a sample of “variable galaxies”, i.e. galaxies with variable nuclei, in the field of Selected Area 57, where other detection techniques were applied, including colors and absence of proper motion (Koo, Kron & Cudworth 1986; Koo & Kron 1988), and for several objects the AGN character was demonstrated either by spectroscopic observations (Trevese et al. 2008) or by X-ray emission (Trevese et al. 2007) (see below).

In many respects, the best way to detect AGNs is just to use X-ray surveys, which enable to discriminate between starlight and accretion-powered sources, such as AGNs. Furthermore, hard (e.g. 2-10 KeV) X-rays are less affected by dust absorption with respect to other bands. The advent of X-ray imaging surveys with Einstein, ASCA, BeppoSAX, and then XMM-Newton and Chandra have permitted to improve dramatically our understanding of accretion powered sources and their cosmic evolution. These surveys provide the evidence of a strong luminosity dependence of the evolution, low luminosity sources (i.e. Seyfert galaxies) peaking at a significantly later cosmic time than high luminosity sources (Hasinger 2003; Ueda et al. 2003; La Franca et al. 2005), at variance with the results of the COMBO-17 survey (Wolf et al. 2003), the redshift of maximum co-moving density ranging from ~ 1 to ~ 0.5 . It is obvious that part of the discrepancy is due to the difficulty of selecting Type 2 (absorbed) AGNs with optical techniques, but, even restricting to Type 1 objects, the discrepancy maintains and there is recent evidence that this is due to the incompleteness of optical techniques in selecting LLAGNs (Bongiorno et al. 2007).

The selection through variability has already permitted to identify objects of intrinsically low X-ray to optical ratio, which may be lost by X-ray surveys (Sarajedini et al. 2003, 2006; Trevese et al. 2007) and, in addition to the contribution they give to the study of the LF evolution, provide information on accretion and/or on star-burst activity.

Repeated observations of the same area of sky permit to detect and study various classes of astronomical objects, like variable stars, supernovae, planetary systems, fast moving objects and AGNs. The Large Synoptic Survey Telescope¹ (LSST) foreseen in 2014 (Ivezic 2007) will address most of these issues and will be able to detect AGNs with high completeness to very faint limits (Green et al. 2007). In the mean time, wide field and deep supernova surveys like ESSENCE (Miknaitis et al. 2007), are already providing data that can be analysed for AGN selection. In this paper we report the AGN detection through variability in one of the fields of the Southern inTernediate Redshift ESO Supernova Search (STRESS) (Botticella et al. 2008) and we discuss the properties of the variability-selected objects. The paper is organized as follows. Section 1 describes the data; section 2 describes the method adopted to select the AGN candidates and the resulting sample; section 3 discusses the optical properties of the AGN candidates; section 4 discusses their X-ray properties and section 5 contains a summary of the results. We adopt throughout the cosmology $H = 75 \text{ km s}^{-1} \text{ Mpc}^{-1}$, $\Omega_M = 0.3$, $\Omega_\Lambda = 0.7$.

2. The STRESS supernova search programme

The detection of variable objects is based on a new analysis of the images of the Southern inTernediate Redshift ESO Supernova Search (STRESS), which is a long term project designed to measure the evolution in cosmic time of the rate of all types of Supernova (SN) events (Cappellaro et al. 2005; Botticella et al. 2008). The supernova search is based on the comparison of images of selected sky fields obtained at different epochs. In general, the temporal sampling of the observations is tuned to the specific goal one wants to achieve. To ensure that all SNe are detected within the time elapsed between the first and the last observation of a given field, the time baseline must be longer than the time for a significant luminosity evolution for all SN types, i.e. as long as 3-4 months. For STRESS, 21 fields were initially selected. They are evenly distributed in right ascension, and have been monitored for about 2 years with an average sampling of one observation every three months. A typical observation run was split in two parts: the search and the follow-up observation of candidates. For the search, two consecutive nights were devoted at the ESO/MPI 2.2 m telescope at ESO, La Silla (Chile). The telescope was equipped with the Wide Field Imager (WFI) and a mosaic of 2×4 CCD detectors of 2048×4096 pixels which image a sky area of $\sim 0.25 \text{ deg}^2$ with an excellent spatial resolution of $0.238 \text{ arcsec/pixel}$. When possible, the first observing night was dedicated to obtaining deep V band exposures for candidate detection while in the second night the same fields were observed through a different filter, B or R, to collect color information both for the candidates and the galaxies. Due to a number of technical, meteorological and scheduling constraints, in many cases it was impossible to maintain this observing strategy. This implies that only in a few cases it was not possible to derive the candidate color. For this reason in the following we consider only the V band exposures and take the candidate colors from another survey, as discussed in section 4. In order to remove detector cosmetic defects, cosmic rays, satellite tracks and fast moving objects, for each field were obtained three frames dithered by 5-10 arcsec, for a total exposure time of 900s or in some cases 600s, as reported in Table 1. For each field the difference between the image to be searched (target image) and a suitable archive frame (template image) was computed. After accurate astrometric and photometric registrations, the most crucial step in this process was the matching of the point spread function (PSF) of the two images. This was done using the ISIS2.1 package (Alard 2000) that, from the comparison of the same sources in the two images, computes a space-varying convolution kernel to degrade the image with the best seeing to match the other one. Variable sources leave residuals in the difference image which have been detected and logged into a catalogue using the *SExtractor* program (Bertin & Arnouts 1996). After various steps of checks in order to remove false detection, residuals of moving objects and variable stars, one is left with a few SN candidates, typically from none to a handful per field. More details on the photometric analysis and the follow up spectroscopic campaign are described in Cappellaro et al. (2005) and Botticella et al. (2008). For the purpose of the present work we only note that, on the basis of the spectra obtained at VLT, about 75% of the supernova candidates were confirmed and almost all of the remaining 25% were found to be AGNs.

The approach to candidate selection was designed to avoid as much as possible any selection bias and in particular nuclear candidates were not excluded a priori. Given that, the intrusion of AGNs is unavoidable. For the purpose of SN search, contamination by variable AGNs was reduced by looking at the long

¹ <http://www.lsst.org>

Table 1. AXAF field observation log

Name of Image	Date (yyyy-mm-dd)	Exposure time (s)	seeing (arcsec)
AXAF_V_19991109	1999-11-09	900	1.08
AXAF_V_19991202	1999-12-02	900	1.12
AXAF_V_19991228	1999-12-28	900	1.15
AXAF_V_20001116	2000-11-16	600	0.92
AXAF_V_20001217	2000-12-17	600	0.93
AXAF_V_20011112	2001-11-12	900	1.03
AXAF_V_20011118	2001-11-18	900	0.84
AXAF_V_20011208	2001-12-08	900	0.95

term variability history of the candidates. Source showing long-term, erratic variability, were excluded from the list of SN candidates. While AGNs represent a contamination of the SN sample, they are just the targets of the present analysis. Thus we flag as possible SN contaminants those objects which present a "single flare". Moreover, we are only interested in nuclear variation. This suggests to use aperture photometry instead of image subtraction, and to adopt a statistical approach for variability detection, which is described in the next section. We note that, as it will be shown in the next section, in our variable source selection optimised for AGN detection down to $V \sim 24$ mag, AGN candidates exceed SN candidates by about 44 times, i.e. we expect a SN contamination of less than 3% which is of minor concern. In principle, we can select AGN candidates in the entire collection of fields monitored by the STRESS programme. As a first step we selected the field named AXAF (after the name of the X-ray AXAF satellite subsequently called Chandra), centred at 03:32:23.7 -27:55:52 (J2000) and covering ~ 0.25 deg².

Table 1 reports the names, the dates and the exposure times of the set of 8 images used in the present analysis, which were collected at the ESO 2.2m telescope with the Wide Field Imager in the AXAF field.

This choice is motivated by the fact that this field overlaps: i) the ESO Imaging Survey (EIS) (Arnouts et al. 2001) containing B,V,R,I photometry and a morphological classification based on the *SExtractor* code ; ii) the COMBO-17 survey (Wolf et al. 2004) containing the photometry in 3 broad and 14 narrow bands and providing a classification of the objects in galaxies, AGNs and stars on the sole basis of their spectral energy distribution (SED); iii) the Chandra Deep Field South (CDFS) survey (Giacconi et al. 2002; Alexander et al. 2003) obtained from X-ray exposures of 1 Ms, which has spectroscopic follow up by Szokoly et al. (2004); iv) the Extended Chandra Deep Field South (ECDFS) survey, consisting of four 16.9x16.9 arcmin² pointings of 250 ks each, flanking the CDFS (Lehmer et al. 2005); v) the GOODS survey, which assembles the data from various catalogues, including the above mentioned ones, providing also optical spectra for a sizable fraction of our sample (most from Giavalisco et al. (2004)).

XMM-Newton observations for a total time of ~ 500 ks and centred on the CDFS are also available (Streblyanska et al. 2004; Dwelly & Page 2006), but they cover only a fraction of the AXAF field, at a slightly shallower depth with respect to the 1Ms Chandra observation.

A V band image of the field is shown in Figure 1, where the fields of the above surveys are also indicated.

In this way it is possible to analyse the properties of the objects selected through variability. In particular X-ray emission and optical spectra, whenever available. Also optical colors and image extension provide valuable information.

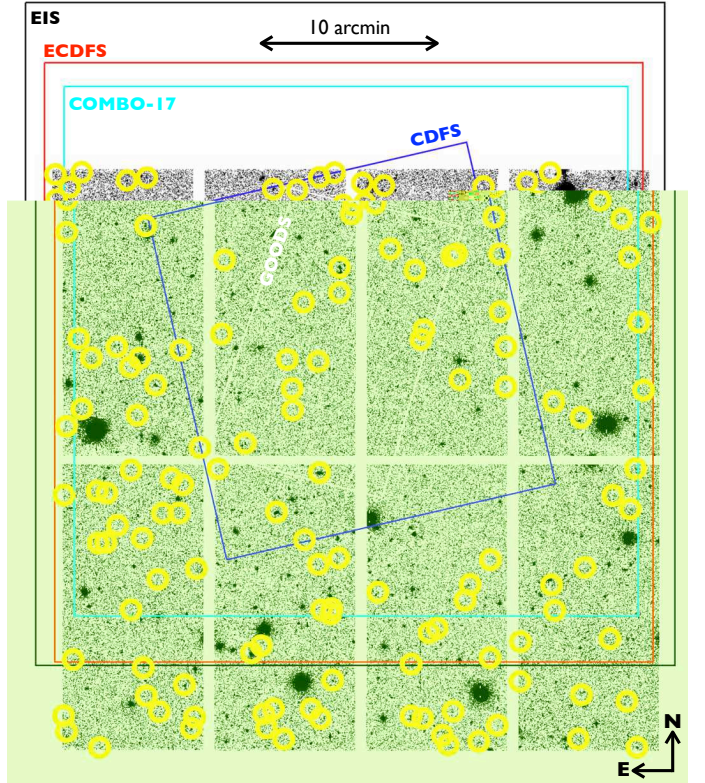


Fig. 1. V band image of the AXAF field taken with the Wide Field Imager at the 2.2m ESO telescope. Contours delimit the area of: i) the ESO Imaging Survey (EIS) (Arnouts et al. 2001) (black); ii) the COMBO-17 survey (Wolf et al. 2004) (cyan); iii) the Chandra Deep Field South (CDFS) 1 Ms survey (Giacconi et al. 2002; Alexander et al. 2003) (blue); the Extended Chandra Deep Field South (ECDFS) 250 ks survey (Lehmer et al. 2005) (red); v) the GOODS survey (Giavalisco et al. 2004). Yellow circles represent the variable objects reported in Table 2.

3. Photometry and selection of variable objects

Objects have been detected with *SExtractor* from each of the 8 images corresponding to the different epochs of observation of the AXAF field. The image AXAF_V_20011208, corresponding to the 8-th epoch (see Table 1), has been selected as reference since it contains the largest number of objects, due to the better image quality, and has also the best overlapping area with the field of the other images. The relevant catalogue was assumed as reference. Aperture photometry was performed for each object on all images at the same (α, δ) positions, and in various apertures.

The V magnitudes, reported in column 4 of Table 2, are scaled to the (AB) system magnitudes, as taken from the EIS catalogue we use for color information. More specifically the zero point of our scale is defined by the condition $\langle V - V_{EIS} \rangle = 0$ where the brackets indicate the average taken over all sources with the following constraints: i) non variable, i.e. $\sigma^* \leq 3$ (see below) ; ii) $17 < V_{EIS} < 21.5$ mag; iii) point-like, i.e. with *SExtractor* stellarity index > 0.9 . The reason for the latter condition is that we used fixed aperture magnitudes, while the EIS catalogue reports "total" magnitudes as measured by *SExtractor*, so that for diffuse objects $V - V_{EIS}$ depends on the extension of the image, thus becoming itself another indicator of stellarity. This can be seen in Figure 2, where stars occupy a "stellar locus" around

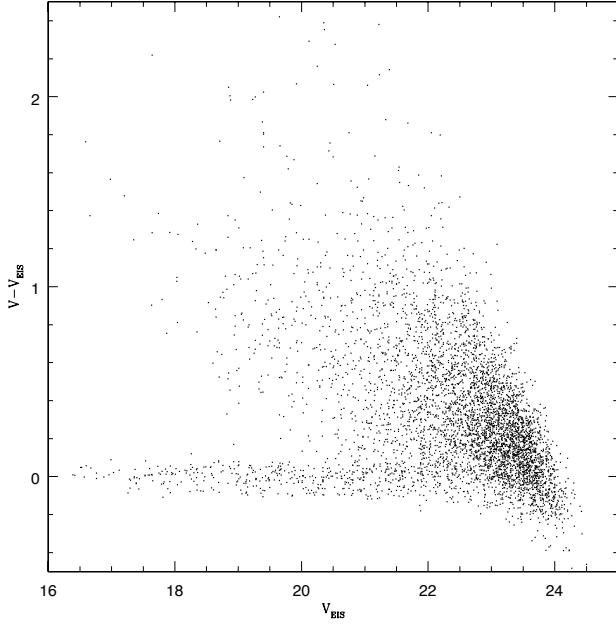


Fig. 2. The difference $V - V_{EIS}$ between the magnitudes we measured on 2.2m WFI images and those reported in the EIS catalogue.

$V - V_{EIS} = 0$ and galaxies are spread over the upper part of the plot. The r.m.s. dispersion of the stellar locus provides an indication of the (quadratically) combined photometric uncertainties of our and EIS magnitudes which are 0.048, 0.056 and 0.11 for $17 < V_{EIS} < 19$, $19 < V_{EIS} < 21.5$ and $21.5 < V_{EIS} < 22.5$ respectively. The completeness limit of our catalogue is about $V = 24$.

Given any image pair (i,j), we compute the mean square difference $\langle (m_i - m_j)^2 \rangle \equiv \Sigma_{i,j}^2 = \Sigma_i^2 + \Sigma_j^2$ between the magnitudes of all objects at two epochs (i,j), where the angular brackets represent the ensemble average on the objects and Σ_i and Σ_j denote the photometric noise of each image and we neglect the contribution of intrinsically variable objects, since they represent a small fraction of the objects in the field. Of course the photometric noise and the optimal aperture depend on the observing conditions and on the magnitude of the object. However in practice the above dependence is not very strong. Thus, for simplicity, we adopted a fixed aperture of 4 pixel (0.92 arcsec) radius, for all magnitudes and epochs.

Indicating with m_k^o the magnitude of the k-th object on the reference image, and with m_k^i the magnitude of the same object on i-th image, and denoting with $d^{(i,o)} \equiv \langle m_k^i - m_k^o \rangle$ the ensemble average in a given magnitude bin, we computed the relative magnitudes $\mu_k^i(m) \equiv (m_k^i - m_k^o) - d^{(i,o)}$, for each object k and each epoch i. The amplitude of the magnitude bins was the result of a trade-off between the number of objects in each bin and the necessity of tracing the dependence of $d^{(i,o)}$ on m. The computation of the ensemble was iterated after a 3- Σ clipping to minimize the effect on $\mu_k^i(m)$ of the most deviant points, which likely correspond to intrinsic variations rather than noise fluctuations.

In this way we obtained, for each object in the field, relative light curves which are independent of the observing condition (exposure, background light, seeing, CCD amplification).

Finally, from the light curve of each object k, we compute the mean \bar{m}_k and the r.m.s. deviation σ_k :

$$\bar{m}_k = \frac{1}{N_{epo}} \sum_i m_k^i, \quad \sigma_k = \left[\frac{1}{N_{epo}} \sum_i (m_k^i - \bar{m}_k)^2 \right]^{1/2}, \quad (1)$$

where N_{epo} is the number of epochs, which in our case is 8, or smaller in the case of some objects, close to the border, which at some epoch fall off the field or are contaminated by hot pixels or other defects. In any case we decided to consider only objects having measured magnitudes in at least 5 of the 8 epochs of observation. This way about 2% of the objects is lost and our final reference catalogue contains 7267 objects brighter than $V = 24$. Figure 3 shows $\sigma \equiv \sigma_k$ (hereinafter we omit the k subscript for simplicity) versus the V magnitude for all the objects in our catalogue. It is evident a dependence on V of both the average $s(V) = \langle \sigma \rangle$ and the r.m.s. deviation $\Sigma_\sigma(V) = \langle [\sigma - s(V)]^2 \rangle^{1/2}$, where the average is computed in bins of V. The average $s(V)$ represents the r.m.s. noise which must be subtracted from σ to measure the intrinsic variability. Increasing the number N_{epo} of observations, $s(V)$ does not vary, rather it converges to the r.m.s. noise. Instead, the σ of intrinsically variable objects may or may not change, depending on how the intrinsic variability time scale compares with the total duration of the observing campaign and the sampling intervals. The r.m.s. deviation $\Sigma_\sigma(V)$, instead, decreases as $N_{epo}^{-1/2}$, and thus increasing the number of observations allows to decrease the threshold which defines variable objects. To keep small enough the number of spurious variables produced by the photometric noise, we adopt a $3\text{-}\Sigma_\sigma$ threshold:

$$\sigma \geq [s(V) + 3\Sigma_\sigma(V)]. \quad (2)$$

The continuous line in Figure 3 represents the adopted threshold. σ is a measure of the average amplitude of magnitude changes, which are due in part to photometric noise and in part to intrinsic variability. We can also define for each object a normalized r.m.s. deviation (as in Bershadsky, Trevese & Kron (1998)):

$$\sigma^* \equiv \frac{\sigma - s(V)}{\Sigma_\sigma(V)}, \quad (3)$$

which provides a measure of the significance of the variability. Thus variable objects are defined by the condition $\sigma^* \geq 3$.

From the above discussion it is clear that this method is not optimal for supernova detection. For instance, if the sampling interval between two observations is comparable or larger than the time scale of SN decay, then σ decreases with the number N_{epo} of observing epochs. For AGNs, instead, σ increases on average, at least for delays up to ~ 50 years, as shown by the structure function analysis of AGN variability (de Vries, Becker & White 2004; de Vries et al. 2005).

Our procedure, once applied to the entire AXAF field, produces a list of 132 candidates reported in Table 2. A spectroscopic follow up is necessary in any case, not only to confirm the AGN nature of the candidates and exclude other kinds of variable objects, but also to measure their redshift and to assign them to specific classes, like type 1 or 2 Seyfert galaxies, QSOs, low luminosity AGNs, or star-burst galaxies.

The threshold adopted has been chosen as a trade off between the completeness we want to reach and the fraction of spurious candidates (purity or reliability) we are willing to accept in a follow-up spectroscopic campaign. Purity and completeness will be discussed in sections 4 and 5 respectively.

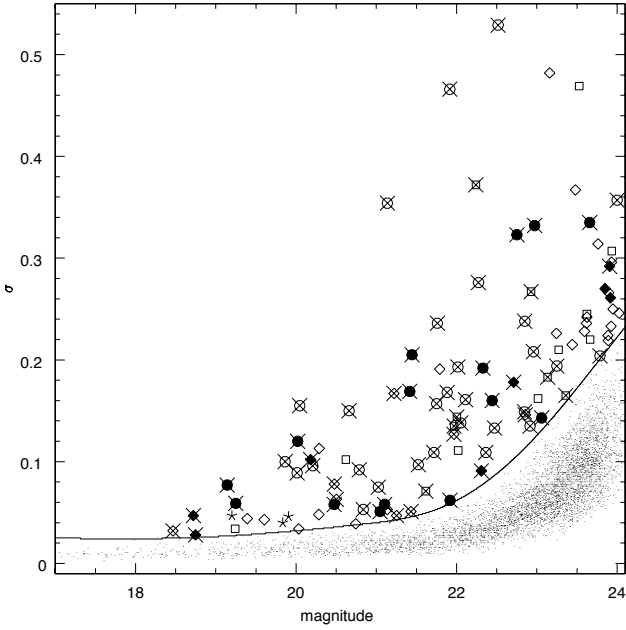


Fig. 3. The r.m.s. magnitude variations $\sigma(V)$ as a function of the apparent V magnitude, for all of the objects in the field. Non variable objects are shown as small dots. Symbols representing the classification are not reported below the $3\text{-}\sigma$ variability threshold, which is indicated by the continuous line. Variable objects, above the variability threshold, are indicated as follows. Filled symbols: objects with spectroscopic redshift; empty symbols: objects without spectroscopic redshift; crosses: X-ray detected objects; circles, diamonds, stars: objects classified by COMBO-17 as QSOs, galaxies, stars, respectively; squares: objects outside the COMBO-17 field.

4. Variability-selected AGN candidates

In Table 2 we report the total sample of variable objects, i.e. objects with $\sigma^* > 3$. Columns have the following meanings: *Column 1*: object identification No.; *Columns 2 and 3*: right ascension α and declination δ (J2000); *Column 4*: V magnitude of present work (rescaled to V_{EIS}); *Column 5*: the standard deviation of the light curve σ ; *Column 6*: the normalised standard deviation σ^* (Eq. 3); *Column 7*: EIS-name; *Columns 8-11*: U, B, V, R from EIS catalogue (AB system); *Column 12*: stellarity index from EIS catalogue S_{EIS} ; *Column 13*: COMBO-17 name; *Column 14*: COMBO-17 (SED) class; *Columns 15*: spectroscopic redshift; *Columns 16*: notes on the nature of the object; *Column 17*: X-ray identification (# in Lehmer et al. (2005) unless otherwise noted); *Columns 18*: X-ray flux (2-8 keV), from Lehmer et al. (2005) unless otherwise noted.

The color-color diagram of Figure 4 shows all 5138 objects with EIS photometry in the AXAF field, measured at 5 epochs at least. Large symbols represent variable objects reported in Table 2, possessing EIS photometry in the relevant bands. All the latter objects (but one) belong to the ECDFS area (see Figure 1). Since the fraction of area covered by EIS and not by COMBO-17 is small (see Figure 1), most objects possess a COMBO-17 classification. More specifically, only 10 objects, represented as open squares, do not possess this classification: 4 of them are detected in X-rays (crosses). Although spectroscopy is eventually necessary to measure their redshifts and to obtain more detailed classifications, the latter objects can be considered AGNs

on the basis of the presence of both variability and X-ray emission (see Maoz et al. 2005). Moreover, we can consider their X-ray to optical ratio (X/O), defined on the basis of the R band optical flux and 2-8 keV X-ray flux, which is less affected by obscuration than softer X-ray bands. All of these objects have $\log X/O > -1$, a value more consistent with AGN activity rather than starburst galaxies, which typically have $\log X/O < -1$ (e.g. Georgakakis et al. 2007). Obviously the opposite is not true, since the host galaxy light may reduce the apparent X/O ratio of a faint AGN, depending also on the aperture adopted for optical photometry and the seeing conditions. The other objects represented by open symbols are either QSOs (circles) or galaxies (diamonds), with COMBO-17 classification but without optical spectroscopy. All of the former are also X-ray emitting and, if we consider the high reliability of the COMBO-17 classification in the case of objects dominated by the nuclear emission, we can assume that they are *bona fide* QSOs.

Among the variable objects classified as galaxies by COMBO-17 and without spectroscopic redshift (open diamonds), some (7) have also X-ray emission and likely they are relatively faint AGNs hosted by a galaxy whose light swamps the nuclear radiation. This is indicated also by their stellarity index in Fig. 5 where most of them (6/7, open diamonds with crosses) are non stellar. The same can be true for the objects which are not detected in X-rays, although in this case the nuclear component must be even fainter. Their variability still suggests the AGN character which, however, requires a spectroscopic confirmation. If the redshift is known, an X-ray luminosity $L_X(2\text{-}8\text{ keV}) > 10^{42}\text{ erg s}^{-1}$ can be assumed as a more direct indication of the AGN character. All of the spectroscopically confirmed QSOs (14 filled circles) have X-ray emission. Of the galaxies with known redshift (8 filled diamonds), 4 show broad emission lines, they are also detected in X-rays, and are consistent with AGN activity.

In summary, to evaluate the purity of the sample, we consider the 104 variable objects in the field covered by X-ray data, 4 of which are variable stars (with a variability in the range 0.03-0.05 mag r.m.s). Among these 104 variable objects, we consider as *bona fide* AGNs: 44 COMBO-17 QSOs with X-ray emission, 4 Combo-17 galaxies with broad emission lines, 8 COMBO-17 galaxies without spectrum but with $\log X/O > -1$, and 7 objects without combo classification but with $\log X/O > -1$. This gives a purity of at least 60% (63/104). We stress that this is a lower limit, since most of the remaining variable objects could also hide some, possibly low-luminosity, AGN component that future spectroscopy could reveal.

In Figure 5 the normalised r.m.s. variability σ^* is reported versus the *SExtractor* stellarity index which, we remind, ranges from 0 (extended objects) to 1 (pointlike objects). Small dots are non variable sources ($\sigma^* \leq 3$). Most QSOs, either or not spectroscopically confirmed, tend to have high values of the stellarity index, but sometimes between 0.6 and 0.8 and not necessarily very close to 1.0. This indicates that often the “fuzz” due to the host galaxy is detected by the stellarity index. However for 2 COMBO-17 QSOs, one of which is spectroscopically confirmed, the stellarity index is typical of a galaxy. This circumstance deserves further investigation. One possible explanation is related with variability: e.g. the nucleus could have been fainter at the epoch of morphological classification and brighter at the epoch of COMBO-17 SED classification. The same is true for objects classified as COMBO-17 galaxies showing a stellarity index close to 1. It appears that all the 4 galaxies with optical spectroscopy (filled diamonds) and stellarity index greater than 0.5 are X-ray emitting and spectroscopically confirmed AGNs.

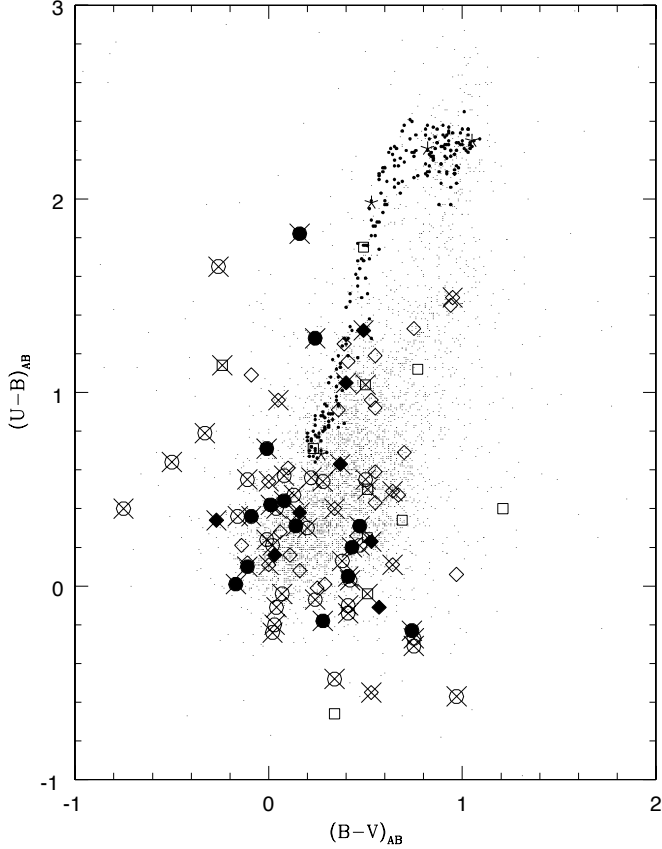


Fig. 4. $(U-B)_{AB}$ versus $(B-V)_{AB}$ colors for all 5138 objects with EIS photometry in the AXAF field and measured at 5 epochs at least. Non-variable galaxies: small dots; non-variable stars: larger dots. Variable objects are indicated as follows. Filled symbols: objects with spectroscopic redshift; empty symbols: objects without spectroscopic redshift; crosses: X-ray detected objects; circles, diamonds, stars: objects classified by COMBO-17 as QSOs, galaxies, stars, respectively; squares: objects outside the COMBO-17 field.

4.1. Comparison with an HST variability survey

A variability survey with Hubble Space Telescope (HST) Advanced Camera for Surveys (ACS) has been undertaken by Klesman & Sarajedini (2007) in the GOODS-South field, which is included in our AXAF field. The variability of a composite sample, consisting of 22 mid-IR power-law sources from Alonso-Herrero et al. (2006) and 104 X-ray sources from Alexander et al. (2003), has been analysed on the basis of ACS exposures at 5 different epochs separated by 45 days intervals. The ACS analysis is motivated by the special interest of detecting and studying LLAGNs. In fact, with the high angular resolution of HST it is possible to perform photometry with a very small aperture: $0.075''$ radius in this case. This reduces the diluting effect of the host galaxy light on the nuclear variability, allowing for its detection down to a nuclear magnitude $M_B \sim -15$, as discussed by Sarajedini et al. (2003). Klesman & Sarajedini (2007) define a variability measure by the standard deviation σ of the light curve, as in the present work, and define the error on the variability measure σ as $\text{error}_\sigma = \sqrt{\Sigma(\text{error}_{mag})^2/N}$, where N is the number of epochs in which the object has been observed and error_{mag} is the formal photometric error on the

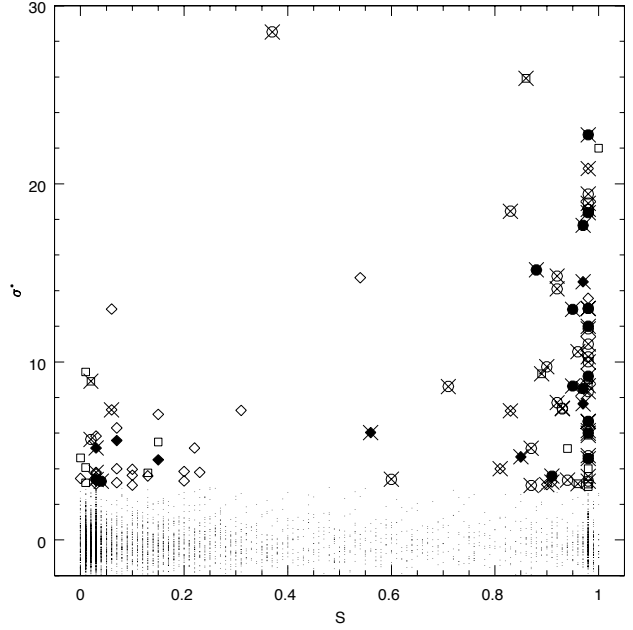


Fig. 5. Normalised r.m.s. variability σ^* versus the *SExtractor* stellarity index S . Symbols as in Figures 3 and 4.

magnitude at each epoch. Though not identical, the definition of error_{mag} is substantially equivalent to our empirical estimate Σ_σ based on the magnitude spread of non variable objects in each magnitude bin. The significance of variability is then defined as: $\text{Significance} = \sigma/\text{error}_\sigma$. Thus, under the assumption that error_σ and our Σ_σ coincide (see Eq. (3)), the relation $\text{Significance} = \sqrt{(\sigma^*)^2 + 1}$ would hold. Notice, however, that the level of noise is not the same in our WFI observations and in the ACS observations of Klesman & Sarajedini (2007).

We can compare our data with the ACS variability observations, for all the objects in common. For these objects Figure 6 shows the Significance versus the nuclear magnitude V_{nuc} taken from Table 1 of Klesman & Sarajedini (2007).

Objects which appear variable in our survey, i.e. with $\sigma^* \geq 3$, are marked by large open circles. For $V_{nuc} < 23.5$, 11/15 (73%) objects which are variable according to Klesman & Sarajedini (2007), i.e. with $\text{Significance} > 3$, are variable in our survey too. This fraction increases to 11/12 (92%) if we restrict to objects with $\text{Significance} > 5$.

Both limits depend on photometric noise. A nuclear magnitude $V_{nuc} = 23.5$ corresponds, on average, to a value of about 23 in our aperture magnitude scale, where the $3-\sigma$ threshold becomes of the order of 0.1 mag (see Figure 3). Moreover, the lower angular resolution of ground based observations tends to dilute nuclear variations increasing the flux variability threshold, for a given significance. In Figure 6 there are two objects which appear variable in our survey but lie below the Significance threshold for Klesman & Sarajedini (2007) dotted line in Figure 6. One of them is an X-ray detected and spectroscopically confirmed QSO with $V_{nuc} = 24.43$ (ID 115 in Table 2). The second (ID 5) is a galaxy with an extra-nuclear Ultra-Luminous X-ray source (ULX) (Hornschemeier et al. 2004; Lehmer et al. 2006), which could cause extranuclear variability, lost by the small-aperture nuclear photometry of Klesman & Sarajedini (2007). In any case WFI and ACS observations were performed in different periods, and for a total sampling time of 0.5 years in the case of

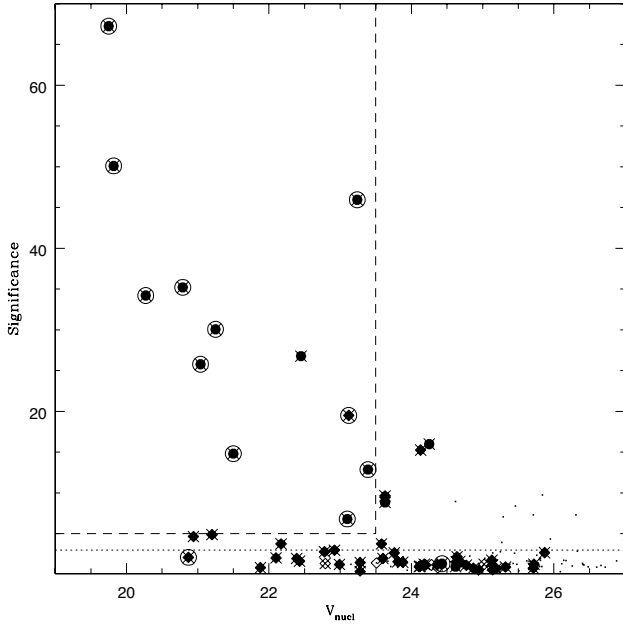


Fig. 6. Significance vs the nuclear magnitude V_{Nucl} from Klesman & Sarajedini (2007). Small dots: objects not in our survey; large symbols: objects which appear in the present survey; filled symbols: objects with spectroscopic; open symbols: objects without spectroscopy; diamonds: galaxies from COMBO-17; circles: COMBO-17 QSOs; crosses: X-ray sources; large open circles: variable objects from our survey. Two of the latter are not variable according to Klesman & Sarajedini (2007) (see text). The horizontal dotted line is the variability threshold of Klesman & Sarajedini (2007). Within the area delimited by the dashed lines, all objects but one are variable according to both surveys.

Klesman & Sarajedini (2007) and 2 years in our case. Thus it is not surprising that a few objects are detected as variable in one survey and not in the other.

4.2. X-ray properties

The X-ray emission is a specific signature of AGNs. The CDFS 1 Ms (Giacconi et al. 2002) is one of deepest X-ray exposures available in the sky. Additional 1 Ms observations of the CDFS have been completed recently² and a further analysis of the field including these data and forthcoming new optical spectra is in progress (Boutsia et al. 2008a). Thus the AXAF field is ideal for a combined study of the X-ray and optical properties of AGNs. In the following we define X/O as the ratio between the observed fluxes in the R optical band and in the 2-8 keV X-ray band. In doing this we neglect the k-correction which however acts in the same sense in both the optical and the X-ray band. Thus effectively we are neglecting a difference in k-corrections which is relatively small with respect to the intrinsic spread of the X/O values.

Due to the very low limiting flux, of about $3 \times 10^{-16} \text{ erg cm}^{-2} \text{ s}^{-1}$ in the 2-8 keV band, the distribution of the optical vs. X-ray fluxes, shown in Figure 7, differs from previous studies with brighter X-ray limits. In fact, below $\sim 5 \times 10^{-15} \text{ erg cm}^{-2} \text{ s}^{-1}$ a

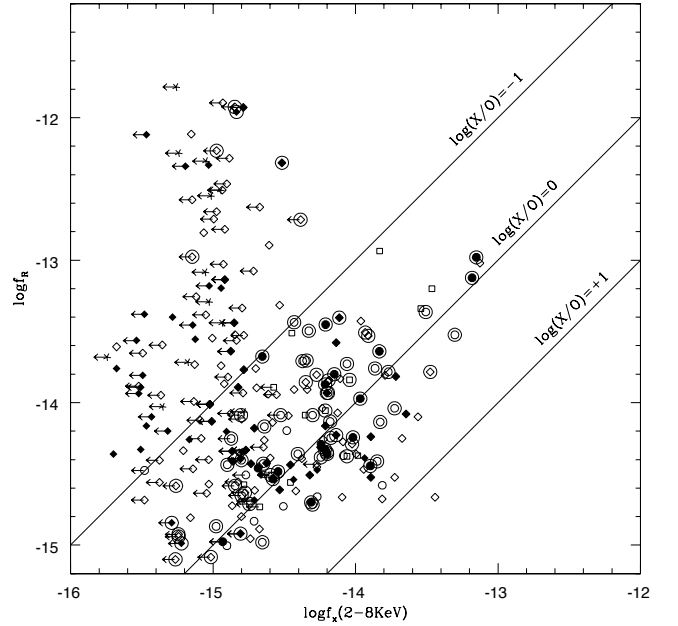


Fig. 7. $\log f_R$ vs $\log f_X(2-8 \text{ keV})$ for all the objects with measured X-ray flux or with estimated upper limit. Fluxes are taken from Lehmer et al. (2005) when available or from Alexander et al. (2003) or Giacconi et al. (2002) otherwise. Symbols as in Figure 3. Variable objects are marked by large open circles. Arrows indicate available 3- σ upper limits from the same surveys, or from our estimates, for objects undetected in the (2-8 keV) band.

population of very low X/O objects appears. This is essentially due to the X-ray emission of normal galaxies. Notice also 12 objects, classified as COMBO-17 stars, lying in the same X-ray flux range, and having $-4 \leq \log(X/O) \leq -1$.

The majority of variable objects (large circles) are concentrated in the $-1 < \log(X/O) < +1$ stripe in Figure 7, as typical AGNs. However 6 variable objects have lower X/O values. All of them have COMBO-17 SEDs of normal galaxies (diamonds). Two of these objects (ID 4 and 5 in Table 2) are detected in X-rays, have low $\log(X/O)$ (-2.2 and -2.9) and both correspond to extranuclear X-ray sources (Hornschemeier et al. 2004; Lehmer et al. 2006). For all the X-ray undetected variable objects we have calculated 3- σ upper limits on the X-ray flux, from the 1Ms Chandra images, if not already available from Lehmer et al. (2005) or Alexander et al. (2003). All the upper limits, for variable and non variable objects, are indicated by leftward arrows in Figure 7. The lowest upper limit on $\log(X/O)$ for variable objects is ≈ -3 and corresponds to the object ID 3.

For objects of known redshift, we can consider the optical vs. X-ray luminosity distribution, shown in Figure 8. There are 18 objects which are classified as COMBO-17 QSOs, and all of them are broad line AGNs according to Szokoly et al. (2004). Most of them (15/18) are variable. Including also COMBO-17 galaxies, there are 23 variable objects, the majority of which (19/23) have a measured X-ray luminosity $L_X(2-8 \text{ keV}) > 10^{42} \text{ erg s}^{-1}$, a value usually assumed to discriminate AGN and normal galaxy emission. Most of the latter objects lie in the stripe $-1 < \log(X/O) < +1$. Notice that 4 of them (21%) were classified as COMBO-17 galaxies but show an emission line spectrum of broad line AGNs (ID 23, 75, 83, 125). Two of them (ID

² <http://xc.harvard.edu/cda/whatsnew.html#cdfs2000-2007>

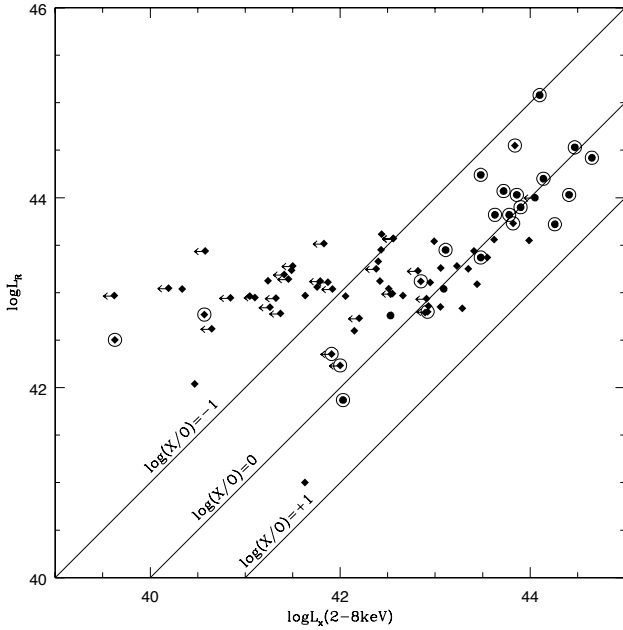


Fig. 8. $\log L_R$ vs $\log L_X(2 - 8 \text{ keV})$ for the objects with known redshift. Symbols as in Figure 7.

75, 125) have relatively low *SEtractor* stellarity index, and thus would be lost by usual color technique, probably due to the relevance of the host galaxy light. Of the 4 variable objects below $10^{42} \text{ erg s}^{-1}$, 2 are the above mentioned ULXs, and the other 2 have upper limits consistent with normal AGNs.

5. Discussion and summary

As discussed in the introduction, the discovery of AGN variability is even older than the concept of AGN itself, and various samples have been created on the basis of this selection technique. However the amplitude of variability depends on the time scale, on the type of object and on its luminosity. Thus the properties of the selected sample, as completeness, purity and the type of detected objects, depend on the sampling interval, on the number of observing epochs, on the total duration of the observing campaign, on the observing band, on the photometric accuracy. The main goal of the present work is to analyse the properties of a sample of AGN candidates selected by variability from a photometric campaign whose sampling rate and duration have been specifically chosen for the detection of Supernovae. In fact, large SN surveys are (and will be) conducted in view of their crucial importance primarily in constraining the dark matter/energy of cosmological models, but also the evolution in cosmic time of the galaxy population. The creation of large statistical samples of AGNs as a by-product of SN surveys may add scientific value to these surveys without increasing their cost in terms of observing time or special requirements. To demonstrate this, we have selected from the STRESS survey a field which has been observed for 8 times during 2 years, and which was studied in detail by various other surveys, including the 1 Ms X-ray survey of the CDFS. As discussed in section 4, our $3\text{-}\sigma$ variability selection produces a sample of good purity, with a number of “true” AGNs about 60% of the total number of AGN candidates. This is a lower limit since a fraction of the unconfirmed candidates may also be AGNs. The completeness of the present

sample, estimated considering only objects with known spectra and X-ray luminosity $L_X(2 - 8 \text{ keV}) \geq 10^{42} \text{ erg s}^{-1}$, is $\sim 44\%$ (19/43, see figure 8), which might increase with further spectroscopic observations (Boutsia et al. 2008a). A relatively high incompleteness suggests caution in basing evolutionary studies on a single selection technique. Still, variability selection may complement the most common surveys based on optical colors or X-ray emission, which suffer different biases.

We stress that increasing the photometric accuracy and the sampling rate, variability surveys can reach much higher completeness. For instance Sesar et al. (2007) obtain $\sim 90\%$ completeness with a threshold of 0.03 mag r.m.s for objects brighter than $g=19.5$, keeping the contamination of the sample at an acceptable level. A survey conducted with the forthcoming LSST may reach virtually 100% completeness at a limiting magnitude $i < 24$, with 12 exposures distributed in one year, according to numerical simulations (Green et al. 2007) based on the extrapolation of statistical properties of AGN variability, as quantified by vanden Berk et al. (2004) from a variability study conducted on a sample of ~ 25000 QSOs observed by the SDSS. We notice also that, despite variability is one of the main characteristics of active nuclei, its nature is still poorly understood. Completely different models have been suggested, including supernova explosions, microlensing and accretion disk instabilities (Arexaga et al. 1997; Hawkins 1993; Kawaguchi et al. 1998; Trevese & Vagnetti 2002). A comparison of models is discussed in Hawkins (2007). Multi-band variability studies of statistical AGN samples can further constrain the physical origin of luminosity changes.

In general, objects which appear as galaxies, due to their extended images or their SEDs, are lost by the color technique (see Figure 4). This happens in the case of LLAGNs, swamped by the host galaxy light. To reach the lowest possible luminosity limit, variability must be studied with the highest possible spatial resolution, as done with HST images both in the HST-N and in the Groth strip fields by Sarajedini et al. (2003, 2006) respectively, in order to reduce the dilution of the nuclear light. Atmospheric seeing obviously prevents reaching the same luminosity limits with ground-based observations. The comparison, presented in section 4.1, among our data, based on ~ 15 min exposures at the ESO 2.2 m telescope, and the variability study of Klesman & Sarajedini (2007) based on ACS/HST images of X-ray selected AGNs, shows that we detect variability at $3\text{-}\sigma$, down to $V_{\text{nuc1}} \sim 23.5$, for $\sim 70\%$ of the objects detected as $3\text{-}\sigma$ variables by these authors. Among these objects, the faintest we observe as $3\text{-}\sigma$ variable has $V_{\text{nuc1}}=24.43$, while the analysis of Klesman & Sarajedini (2007) detects variability down to $V_{\text{nuc1}} \sim 27$. However the area covered by a single field of STRESS is about 900 arcmin^2 . The STRESS project covers 16 fields, thus it can provide about 16 times the 130 variable candidates of the present study, i.e. ~ 2000 , of which about 1200 are expected to be *bona fide* AGNs due to the high purity ($\sim 60\%$) of our sample. This number would allow us to assess statistically the selection effects by comparison with color-selected or X-ray-selected samples. As shown in a previous paper (Trevese et al. 2008), where we analysed the X-ray and optical properties of variability selected objects in SA 57, several “variable galaxies” are NELGs for which it was impossible to assess the starburst or LINER nature, due to insufficient wavelength coverage. Being variable, these objects are interesting in both cases. In fact, if they are LINERs, their variability would strongly support the AGN nature of this kind of objects, following the argument of Maoz et al. (2005), according to which the observed variability cannot be accounted for by luminosity changes of B

stars. Notice that this is *a fortiori* true if we consider longer wavelengths instead of the UV discussed by Maoz et al. (2005), despite the shallow decrease of nuclear variability with redshift (Giallongo, Trevese & Vagnetti 1991; Trevese et al. 2001; vanden Berk et al. 2004). If instead our objects turn out to be starburst galaxies, the origin of their variability would pose a new interesting problem, as in the case of the objects ID 4 and ID 5 in Table 2, which show evidence of extranuclear emission possibly related to ULXs (Hornschemeier et al. 2004; Lehmer et al. 2006).

We note that, from the data so far collected by the ESSENCE supernova survey, in 32 fields for a total area of 8 deg², it would be possible to select on the basis of variability about 4,000 candidates (Boutsia et al. 2008b), which would definitely increase the number of variable NELGs available to increase our knowledge about the relation between the starburst and AGN phenomenon, and providing another example of synergic SN/AGN survey (cf. the conferences on this subject, Bono, Castellani, & Trevese 2003; Trevese & Vagnetti 2004).

Finally, the ~520 arcmin² field of the Large Binocular Camera (Giallongo et al. 2008) at both red and blue arm of the Large Binocular Telescope, which is at present the widest field available for an 8m class telescope, will provide an unprecedented opportunity for deep synergic SN/AGN surveys.

Acknowledgements. We acknowledge B. Leibundgut and R. Nesci for discussions. This work was partly supported by MIUR under grant PRIN 2006/025203. K.B. acknowledges support by ESO studentship program. This research has made use of the NASA/IPAC Extragalactic Database (NED) which is operated by the Jet Propulsion Laboratory, California Institute of Technology, under contract with the National Aeronautics and Space Administration.

References

- Alexander, D. M., Smail, I., Bauer, F. E., Chapman, S. C., Blain, A. W., Brandt, W. N., & Ivison, R. J. 2005, *Nature*, 434, 738
- Alonso-Herrero, A., et al. 2006, *ApJ*, 640, 167
- Anderson, S.F. et al., 2001, *AJ*, 122, 503
- Aretxaga, I., Cid Fernandes, R., & Terlevich, R. 1997, *MNRAS*, 286, 271
- Arnouts, S. et al. 2001, *A&A* 379, 740
- Bertin, E. & Arnouts, S. 1996, *A&AS*, 117, 393
- Boyle, B. J., Shanks, T., Croom, S. M., et al., 2000, *MNRAS*, 317, 1014
- Bershady, M. A., Trevese, D., & Kron, R. G. 1998, *ApJ*, 496, 103
- Bongiorno, A., Zamorani, G., Gavignaud, I. et al. 2007, *A&A*, 472, 443
- Botticella, M. T., Riello, M., Cappellaro, E. et al., 2008, *A&A* 479, 49
- Bono, G., Castellani, M., & Trevese, D. Eds., 2003, *Variability with Wide-Field Imagers*, Mem.SAIt, 74, 851
- Boutsia et al. 2008a, in preparation
- Boutsia et al. 2008b, in preparation
- Cappellaro, E., Riello, M., Altavilla, G., et al. 2005, *A&A* 430, 83
- Cristiani, S., Vio, R., Andreani, P. 1990, *AJ* 100, 56
- Cristiani, S. et al. 1996, *A&A*, 306, 395
- Croom, S.M. et al. 2001, *MNRAS* 322, L29
- de Vries, W.H., Becker, R.H., & White, R.L. 2003, *AJ* 126, 1217
- de Vries, W.H., Becker, R.H., White, R.L., & Loomis, C., 2005, *AJ*, 129, 615
- Dwelly, T., & Page, M.J., 2006, *MNRAS*, 372, 1755
- Fan et al., 2001, *AJ*, 121, 54
- Geha, M., Alcock, C., Allsman, R. A., et al. 2003, *ApJ* 125, 1
- Georgakakis, A., Rowan-Robinson, M., Babbedge, T.S.R., & Georgantopoulos, I. 2007, *MNRAS* 377, 203
- Giacconi, R., Zirm, A., Wang, J. 2002, *ApJS* 139, 369
- Giallongo, E., Ragazzoni, R., Grazian, A. et al., 2008, *A&A*, 482, 349
- Giallongo, E., Trevese, D., & Vagnetti, F., 1991, *ApJ*, 377, 345
- Giavalisco, M., Ferguson, H.C., Koekemoer, A.M. 2004, *ApJ*, 600, 93
- Grazian, A., Fontana, A., de Santis, C. et al., 2006, *A&A* 449, 951
- Green, R.F., Brandt, W.N., vanden Berk, D.E., Schneider, D.P., Osmer, P.S. 2007, *ASP Conf. Ser.* 373, 707
- Hasinger, G., 2003, *AIP conf.*, 666, 227
- Hawkins, M. R. S., 1983, *MNRAS*, 202, 571
- Hawkins, M. R. S., 1993, *Nature*, 366, 242
- 2007, *A&A*, 462, 581
- Hook, I. M., McMahon R. G., Boyle, B. J., & Irwin, M. J. 1994, *MNRAS*, 268, 305
- Hornschemeier, A.E., Alexander, D.M., Bauer, F.E., et al. 2004, *ApJLett* 600, L47
- Ivezic, Z. 2007, *AAS* 210, 66.05
- Jiang, L., Fan, X., Ivezic, Z., et al. 2007, *ApJ* 656, 680
- Kawaguchi, T., Mineshige, S., Umemura, M., & Turner, E. L. 1998, *ApJ*, 504, 671
- Klesman, A., & Sarajedini, V., 2007, *ApJ*, 665, 225
- Kellermann, K. I., Sramek, R., Schmidt, M. 1989, *AJ* 98, 1195
- Koo, D. C., Kron, R. G., & Cudworth, K. M. 1986, *PASP* 98, 285
- Koo & Kron 1988, *ApJ*, 325, 92
- La Franca, F., Fiore, F., Comastri, A. et al., 2005, *ApJ*, 635, 864
- Lehmer, B.D., Brandt, W.N., Alexander, D.M., et al. 2005, *ApJS* 16, 21
- Lehmer, B.D., Brandt, W.N., Hornschemeier, A.E., et al. 2006, *AJ* 131, 2394
- Matthews, T.A. & Sandage, A.R., 1963, *ApJ*, 138, 30
- Maoz, D.; Nagar, N.M.; Falcke, H., Wilson, A.S. 2005, *ApJ* 625, 699
- Miknaitis, G. 2007, *ApJ* 666, 674
- Ravikumar, C.D., Puech, M., Flores, H. et al. 2007, *A&A* 465, 1099
- Richards, G. T., Strauss, M. A., Fan, X., et al., 2006, *AJ*, 131, 2766
- Sarajedini, V.L., Gilliland, R.L., & Kasm, C., 2003, *ApJ*, 599, 173
- Sarajedini, V.L., Koo, D.C., Phillips, A.C., et al. 2006, *ApJSupp* 166, 69
- Schmidt, M., 1968, *ApJ*, 151, 393
- Schmidt, M., 1970, *ApJ*, 16, 371
- Schmidt, M., Schneider, D.P., & Gunn, J.E. 1995, *AJ* 110, 68
- Sesar, B., Ivezic, Z., Lupton, R. H. et al., 2007, *AJ*, 134, 2236
- Streblyanska, A., Bergeron, J., Brunner, H., Finoguenov, A., Hasinger, G., Mainieri, V., 2004, *Nuc.Phys.B Proc.Suppl.*, 132, 232
- Szokoly, G.P., Bergeron, J., Hasinger, G., et al. 2004, *ApJSupp* 155, 271
- Trevese, D. & Vagnetti, F., 2002, *ApJ*, 564, 630
- Trevese, D. & Vagnetti, F. Eds., 2004, *Sinergies in Wide-Field Observations*, *Baltic Astro.*, 13, 611
- Trevese, D., Pittella G., Kron R. G., Koo D. C., & Bershadsky M. A. 1989, *AJ*, 98, 108
- Trevese, D., Kron R. G., & Bunone, A. 2001, *ApJ*, 551, 103
- Trevese, D., Kron, R. G., Majewski, S. R., Bershadsky, M. A., Koo, D. C. 1994, *ApJ*, 433, 494
- Trevese, D., Vagnetti, F., Puccetti, S., Fiore, F., Tomei, M., Bershadsky, M. A. 2007, *A&A*, 469, 1211
- Trevese, D., Vagnetti, F., Zitelli, V., Boutsia, K., & Stirpe, G.M., 2008 *A&A* 477, 473
- Ueda, Y., Akijama, M., Ohta, K., Miyaji, T., 2003, *ApJ*, 598, 886
- Usher, P. D. 1978, *ApJ*, 222, 40
- van den Berg, S., Herbst, E., & Pritchett, C., 1973, *AJ*, 78, 375
- Vanden Berk, D.E., Wilhite, B. C., Kron, R. G., et al., 2004, *ApJ*, 601, 692
- Véron, P., & Hawkins, M.R.S., 1995, *A&A*, 296, 665
- Warren, S.J., Hewett, P.C., & Osmer, P.S. 1994 *ApJ* 421, 412
- Wolf, C., Wisotzki, L., Borch, A., et al., 2003, *A&A*, 408, 499
- Wolf, C., Meisenheimer, K., Kleinheinrich, M. et al. 2004, *A&A* 421, 913

Table 2. Catalog of the variable objects

ID (1)	α (J2000) (2)	δ (J2000) (3)	V (4)	σ (5)	σ^* (6)	EIS-name (7)	U_{EIS} (8)	B_{EIS} (9)	V_{EIS} (10)	R_{EIS} (11)	S_{EIS} (12)	COMBO (13)	class ^a (14)	z (15)	notes ^b (16)	XID ^c (17)	f_X (2-8keV) ^c (18)
1	03:33:19.00	-27:41:44.9	16.97	0.031	22.0	J033319.00-274145.2	19.53	17.55	17.02	16.51	1.00	47439	S				
2	03:33:09.36	-28:07:25.7	17.13	0.035	4.6	J033309.36-280725.8											
3	03:33:20.61	-27:49:10.1	18.47	0.032	3.8	J033320.61-274910.3	19.12	17.63	16.68	16.12	0.03	32802	G			664	<1.42e-15
4	03:32:35.09	-27:55:33.0	18.72	0.047	5.2	J033235.09-275533.2	18.58	17.26	16.77	16.21	0.03	18675	G	0.038	LEX,EN	247 ^d	1.46e-15 ^d
5	03:32:29.99	-27:44:04.8	18.75	0.028	3.4	J033230.00-274405.0	18.95	17.90	17.50	17.10	0.03	42499	G	0.076	LEX,EN	392	3.05e-15
6	03:32:27.01	-27:41:05.1	19.14	0.077	13.0	J033227.02-274105.2	19.55	19.13	19.12	19.12	0.98	48284	Q	0.734	BLAGN	379	6.58e-14
7	03:31:16.34	-27:57:34.7	19.20	0.047	4.6	J033116.35-275735.0	20.15	19.47	19.20	18.96	0.98	13879	S				
8	03:32:46.76	-28:08:46.7	19.21	0.055	6.5	J033246.76-280846.8											
9	03:33:38.86	-27:40:16.4	19.24	0.034	3.0	J033338.87-274016.9	21.53	19.78	19.29	18.80	0.98						
10	03:32:08.66	-27:47:34.4	19.25	0.059	9.2	J033208.68-274734.5	19.78	19.07	19.08	18.76	0.98	34357	Q	0.543	BLAGN	305	7.05e-14
11	03:33:16.51	-27:50:39.5	19.39	0.044	4.0	J033316.51-275039.7	19.52	18.33	17.78	17.27	0.07	28467	G				
12	03:32:45.95	-27:57:45.3	19.60	0.043	3.7	J033245.97-275745.6	18.83	17.67	17.26	16.89	0.03	14012	G/U				<1.06e-15 ^e
13	03:33:16.07	-27:39:02.8	19.83	0.040	3.1	J033316.08-273902.9	23.26	20.96	19.91	18.92	0.98	52646	S				
14	03:32:32.00	-28:03:09.9	19.86	0.100	11.9	J033232.02-280310.0	19.65	19.85	19.82	19.72	0.98	2006	Q			398	3.11e-14
15	03:31:54.65	-28:10:35.7	19.88	0.032	5.0	—											
16	03:33:32.52	-27:38:43.9	19.91	0.046	4.0	J033332.53-273844.3	23.03	20.77	19.95	19.15	0.98	53315	S				
17	03:31:14.50	-28:10:54.7	19.93	0.036	3.3	—											
18	03:33:31.37	-27:56:34.2	20.01	0.089	10.0	J033331.39-275634.6	20.72	20.15	20.07	19.90	0.98	15952	Q			723	3.71e-15
19	03:32:26.50	-27:40:35.7	20.02	0.120	17.7	J033226.51-274035.7	20.34	19.98	20.07	19.94	0.97	49298	Q	1.031	BLAGN	375	6.16e-15
20	03:32:11.84	-28:09:11.0	20.03	0.040	6.8	—											
21	03:32:44.16	-27:39:42.1	20.03	0.034	3.3	J033244.16-273942.3	19.95	19.03	18.48	18.10	0.03	51684	G				<4.11e-15 ^f
22	03:33:28.93	-27:56:41.1	20.05	0.155	19.4	J033328.95-275641.4	20.72	20.25	20.12	20.12	0.98	15731	Q			712	4.98e-14
23	03:32:16.20	-27:39:30.2	20.18	0.102	14.5	J033216.21-273930.5	20.74	20.36	20.20	19.82	0.97	51593	G/U	1.324	BLAGN	345	7.69e-15
24	03:33:09.71	-27:56:14.0	20.21	0.096	11.0	J033309.72-275614.3	20.55	20.15	20.11	20.05	0.98	16621	Q			596	4.70e-15
25	03:31:16.69	-27:43:29.6	20.28	0.048	3.5	J033116.70-274329.5	20.34	19.43	19.07	18.78	0.03	43124	G				
26	03:32:34.57	-28:03:14.0	20.29	0.113	13.6	J033234.59-280314.1	20.91	20.30	20.20	20.08	0.98	1821	G/U				
27	03:32:38.12	-27:39:44.9	20.48	0.058	6.0	J033238.14-273945.0	20.89	20.84	20.43	20.41	0.98	50997	Q	0.837	BLAGN	417	1.47e-14
28	03:33:21.09	-27:39:11.8	20.48	0.078	7.3	J033321.09-273912.1	20.50	20.39	20.39	20.14	0.83	52280	G/U			670	1.23e-14
29	03:32:37.29	-28:08:47.0	20.50	0.135	16.6	J033237.32-280847.3											
30	03:33:12.63	-27:55:51.6	20.50	0.063	6.1	J033312.63-275551.9	21.39	20.43	20.38	20.08	0.98	17446	G			611	1.17e-14
31	03:31:11.38	-27:41:31.9	20.62	0.102	9.0	J033111.39-274131.9	20.30	20.96	20.62	20.57	0.98						
32	03:33:22.79	-27:55:23.8	20.66	0.150	18.6	J033322.80-275524.0	20.94	21.04	20.63	20.58	0.98	18256	Q			678	4.25e-15
33	03:32:53.90	-27:53:54.1	20.74	0.039	3.1	J033253.90-275354.3	20.62	19.66	19.13	18.75	0.03	21830	G				<7.14e-16 ^e
34	03:33:26.24	-27:58:29.7	20.79	0.092	10.3	J033326.26-275830.0	20.58	20.69	20.65	20.57	0.98	11941	Q			700	4.54e-15
35	03:32:20.30	-28:02:14.8	20.84	0.053	7.4	J033220.34-280214.8	21.03	21.17	20.76	20.63	0.93	4050	Q			358	8.71e-15
36	03:32:31.78	-28:07:10.4	20.84	0.045	3.6	J033231.81-280710.6											
37	03:33:29.22	-27:59:26.7	21.03	0.075	7.7	J033329.24-275927.1	21.40	21.37	20.95	20.71	0.92	9954	Q/G			716	1.37e-14
38	03:32:39.09	-27:46:01.8	21.05	0.051	4.6	J033239.10-274602.0	21.11	21.29	21.01	20.81	0.98	37487	Q	1.216	BLAGN	423	7.09e-15
39	03:32:44.18	-28:10:28.5	21.07	0.193	24.7	—											
40	03:32:09.44	-27:48:06.8	21.10	0.058	6.7	J033209.46-274806.9	22.94	21.12	20.96	20.50	0.98	33069	Q	2.810	BLAGN	309	2.22e-15
41	03:31:58.13	-28:02:41.5	21.14	0.053	5.8	J033158.14-280241.7	23.02	21.57	20.63	19.73	0.03	3111	G/U				
42	03:31:20.76	-27:56:48.9	21.14	0.354	41.6	J033120.77-275649.2	21.11	20.87	20.88	20.77	0.98	15278	Q			21	1.70e-14
43	03:33:20.01	-27:59:12.4	21.22	0.167	20.9	J033320.02-275912.7	21.80	21.26	21.26	20.92	0.98	10418	G			661	6.46e-15
44	03:31:15.04	-27:55:18.6	21.25	0.047	3.3	J033115.05-275518.8	21.19	21.74	21.21	20.77	0.91	18408	G			7	3.35e-14
45	03:33:07.64	-28:09:51.5	21.27	0.045	3.4	—											

ID (1)	α (J2000) (2)	δ (J2000) (3)	V (4)	σ (5)	σ^* (6)	EIS-name (7)	U_{EIS} (8)	B_{EIS} (9)	V_{EIS} (10)	R_{EIS} (11)	S_{EIS} (12)	COMBO (13)	class ^a (14)	z (15)	notes ^b (16)	XID ^c (17)	$f_X(2\text{-}8\text{keV})^c$ (18)
46	03:33:06.78	-28:09:14.3	21.42	0.186	23.4	—											
47	03:32:29.98	-27:45:29.9	21.42	0.169	18.4	J033229.99-274530.1	21.51	21.41	21.52	21.24	0.98	38551	Q	1.218	BLAGN	391	1.08e-14
48	03:31:35.43	-28:03:15.8	21.43	0.051	3.1	J033135.44-280315.8	22.13	21.73	21.39	20.95	0.90	1647	G/U			94	4.48e-15
49	03:32:59.86	-27:47:48.2	21.45	0.205	22.8	J033259.85-274748.4	22.29	22.09	21.66	21.92	0.98	33644	Q	2.579	BLAGN	526	9.59e-15
50	03:33:10.63	-27:57:48.5	21.52	0.097	10.6	J033310.64-275748.8	21.68	21.47	21.45	21.14	0.96	13332	Q			601	6.41e-15
51	03:32:05.22	-28:04:15.3	21.62	0.071	5.9	J033205.24-280415.5	22.51	22.01	21.50	20.91	0.98					282	9.07e-15
52	03:31:18.69	-27:41:21.4	21.72	0.109	7.4	J033118.71-274121.4	22.18	22.75	21.78	21.53	0.93	47501	Q/G			12	<2.98e-15
53	03:32:01.18	-28:08:54.8	21.74	0.157	16.5	—											
54	03:33:30.93	-28:10:55.5	21.75	0.053	3.5	—											
55	03:31:27.79	-28:00:51.0	21.75	0.157	13.0	J033127.80-280051.2	21.54	21.78	21.76	21.53	0.98	6817	Q			54	5.00e-15
56	03:33:32.75	-27:49:07.8	21.76	0.236	18.9	J033332.77-274908.0	22.23	21.59	22.09	21.64	0.98	31085	Q			728	6.63e-15
57	03:33:05.31	-27:54:09.1	21.79	0.191	14.7	J033305.31-275409.4	22.90	22.21	21.51	21.19	0.54	20787	G		SNC		
58	03:32:11.83	-28:06:16.3	21.82	0.086	6.6	J033211.85-280616.5	21.50		20.68	20.35	0.03			0.274	SN		
59	03:31:29.41	-28:10:27.4	21.87	0.148	10.8	—											
60	03:32:32.28	-28:03:28.3	21.88	0.168	14.1	J033232.30-280328.4	21.85	21.89	21.82	21.41	0.92	1257	Q			400	1.88e-14
61	03:31:36.25	-28:01:49.7	21.92	0.466	36.3	J033136.25-280149.8	22.20	21.80	22.55	22.27	0.97	4809	Q			100	5.71e-15
62	03:32:59.07	-27:43:39.5	21.92	0.062	3.3	J033259.06-274339.8	22.26	21.95	21.48	20.99	0.04	42601	Q/G	0.733	BLAGN	516	6.13e-15
63	03:32:03.89	-28:10:15.6	21.93	0.247	21.9	—											
64	03:33:35.56	-27:39:34.7	21.97	0.127	7.3	J033335.57-273935.1	23.00	22.51	21.87	20.82	0.06	51491	G			741	5.32e-15
65	03:31:44.14	-28:05:00.5	21.97	0.135	8.7	J033144.17-280500.7	23.68	22.64	22.14	21.53	0.98					148	<1.57e-15
66	03:33:19.04	-28:08:02.5	21.99	0.368	33.9	J033319.06-280803.0											
67	03:31:21.45	-28:04:50.5	22.00	0.144	9.3	J033121.47-280450.6	22.87	21.73	21.97	21.45	0.89					26	6.14e-15
68	03:33:06.26	-28:00:55.6	22.02	0.193	14.8	J033306.28-280055.8	22.40	22.19	21.72	21.73	0.92	6735	Q			567	2.29e-15
69	03:31:13.04	-27:50:55.6	22.02	0.111	5.5	J033113.05-275055.8	23.67	22.55	21.78	20.66	0.15			0.540	SN		
70	03:32:30.19	-28:00:19.9	22.05	0.138	9.7	J033230.21-280020.0	22.64	22.08	21.86	21.93	0.90	7902	Q			393	6.70e-15
71	03:33:19.78	-28:06:27.4	22.06	0.075	4.0	J033319.78-280627.8	22.58		22.01	21.09	0.98						
72	03:31:35.78	-27:51:34.9	22.11	0.161	8.3	J033135.79-275134.9	22.41	21.62	21.95	21.65	0.98	25884	Q			96	1.49e-14
73	03:31:51.86	-28:05:54.9	22.24	0.372	25.9	J033151.88-280555.1	22.76		22.46	22.25	0.86					200	8.71e-15
74	03:31:56.86	-28:01:48.7	22.27	0.276	18.5	J033156.88-280149.0	22.57	22.21	22.37	21.94	0.83	4995	Q			235	<1.34e-15
75	03:32:17.14	-27:43:03.3	22.31	0.091	4.7	J033217.15-274303.5	23.16	22.53	22.16	21.14	0.85	43863	G	0.569	BLAGN	348	6.29e-15
76	03:32:00.37	-27:43:19.7	22.33	0.192	12.0	J033200.37-274319.9	22.76	22.99	22.25	22.13	0.98	43151	Q	1.037	BLAGN	250	6.09e-15
77	03:31:51.78	-28:00:25.6	22.37	0.109	4.7	J033151.80-280025.9	22.88	22.58	22.38	22.38	0.98	7671	Q			199	2.25e-15
78	03:31:50.95	-27:41:15.9	22.44	0.160	8.6	J033150.97-274116.1	23.19	22.75	22.67	22.21	0.95	47615	Q	0.253	NELG	192	6.32e-15
79	03:31:17.07	-28:08:20.5	22.45	0.182	8.2	—											
80	03:31:49.41	-27:46:34.2	22.47	0.133	6.6	J033149.42-274634.4	23.26	22.72	22.44	22.40	0.98	36120	Q			181	1.26e-15
81	03:33:00.78	-27:55:20.7	22.52	0.529	28.5	J033300.73-275520.6	22.73	23.00	22.25	22.34	0.37	18324	Q/G			532	1.42e-14
82	03:31:28.61	-28:07:58.6	22.63	0.330	14.7	J033128.61-280759.0											
83	03:31:49.54	-27:43:19.4	22.71	0.178	7.6	J033149.55-274319.6	23.16	22.93	22.40	21.88	0.97	43170	G	1.320	q	184	7.31e-15
84	03:32:10.91	-27:44:15.0	22.75	0.323	15.2	J033210.92-274415.2	23.35	23.04	22.90	22.42	0.88	41159	Q	1.600	BLAGN	316	1.27e-14
85	03:32:48.57	-28:09:50.5	22.84	0.167	5.2	—											
86	03:31:40.04	-27:39:17.8	22.85	0.149	3.4	J033140.06-273917.8	23.10	23.17	22.93	22.94	0.94	51835	Q			119	<1.59e-15
87	03:33:22.85	-28:03:13.0	22.85	0.238	8.6	J033322.87-280313.2	23.15	22.60	22.71	22.32	0.71	1731	Q			679	<1.58e-15
88	03:32:38.87	-27:59:18.7	22.86	0.146	4.0	J033238.88-275918.9	23.33	23.22	22.58	22.04	0.81	10151	G			419	9.43e-15
89	03:31:44.21	-28:07:14.1	22.90	0.219	6.8	J033144.22-280714.4											
90	03:31:49.95	-28:09:41.6	22.91	0.355	14.1	—											

ID (1)	α (J2000) (2)	δ (J2000) (3)	V (4)	σ (5)	σ^* (6)	EIS-name (7)	U_{EIS} (8)	B_{EIS} (9)	V_{EIS} (10)	R_{EIS} (11)	S_{EIS} (12)	COMBO (13)	class ^a (14)	z (15)	notes ^b (16)	XID ^c (17)	$f_X(2-8\text{keV})^c$ (18)
91	03:33:16.08	-28:01:31.3	22.92	0.135	3.4	J033316.10-280131.5	22.38	22.86	22.52	22.21	0.60	5498	Q/G			631	3.94e-15
92	03:33:39.28	-28:10:01.4	22.92	0.150	4.1	—											
93	03:32:49.84	-28:05:14.5	22.93	0.267	8.9	J033249.84-280514.8	23.21		22.64	22.18	0.02					477	6.28e-15
94	03:33:10.19	-27:48:42.0	22.96	0.208	5.1	J033310.19-274842.3	24.27	23.72	23.22	22.77	0.87	31898	Q/G			597	<1.43e-15
95	03:33:15.75	-28:08:55.2	22.96	0.130	3.1	—											
96	03:32:43.24	-27:49:14.1	22.97	0.332	13.0	J033243.25-274914.4	22.54	22.53	22.70	22.65	0.95	30792	Q	1.920	BLAGN	441	2.63e-15
97	03:33:38.93	-27:42:05.3	23.02	0.162	3.2	J033338.94-274205.7	22.63	22.29	21.60	20.98	0.01						
98	03:32:41.86	-27:52:02.5	23.06	0.143	3.6	J033241.86-275202.6		23.79	23.14	22.52	0.91	25042	Q	3.592	BLAGN	435	2.86e-15
99	03:31:14.29	-27:47:07.4	23.13	0.183	3.6	J033114.30-274707.5	23.53	23.57	23.06	22.58	0.98					4	<2.54e-15
100	03:32:08.92	-28:09:18.7	23.15	0.155	3.5	—											
101	03:33:21.21	-27:52:19.6	23.16	0.482	13.0	J033321.22-275219.6	23.60	23.48	23.59	23.49	0.06	24466	G				
102	03:32:34.92	-28:09:19.7	23.17	0.382	11.4	—											
103	03:32:32.50	-27:39:02.4	23.25	0.226	6.3	J033232.52-273902.6	25.41	24.08	23.33	22.89	0.07	52474	G				<1.67e-15 ^e
104	03:33:26.31	-27:48:31.1	23.25	0.194	3.3	J033326.32-274831.3	23.75	24.06	23.31	23.10	0.98	32254	Q			702	4.99e-15
105	03:32:52.32	-28:05:38.2	23.27	0.210	4.6	J033252.37-280538.4			17.64		0.00						
106	03:32:07.32	-28:04:30.7	23.36	0.165	3.2	J033207.34-280430.9		23.93	23.18	23.09	0.96					299	<1.80e-15
107	03:33:35.25	-27:51:57.8	23.44	0.215	3.2	J033335.27-275158.1	24.28	23.85	23.30	22.84	0.07	25213	G				
108	03:33:22.96	-27:49:38.1	23.48	0.367	7.1	J033322.97-274937.5	23.64	23.48	23.37	23.69	0.15	30008	G				
109	03:33:39.15	-27:38:51.3	23.53	0.469	9.4	J033339.14-273852.1	23.23	22.98	22.47	21.60	0.01						
110	03:32:49.24	-28:09:02.9	23.54	0.427	9.9	—											
111	03:33:35.97	-27:48:03.7	23.59	0.228	3.1	J033336.00-274803.9	24.32	23.85	23.18	22.86	0.10	33178	G				
112	03:31:28.83	-27:52:27.5	23.62	0.236	3.3	J033128.84-275227.6	23.95	23.36	22.81	22.94	0.20	24036	G				
113	03:31:24.15	-27:40:19.0	23.62	0.242	3.5	J033124.20-274019.5	23.62	23.56	22.59	22.38	0.00	49662	G				
114	03:33:37.58	-28:06:00.2	23.62	0.245	5.1	J033337.63-280600.6			23.60	22.09	0.94						
115	03:32:01.58	-27:43:27.0	23.66	0.335	8.5	J033201.59-274327.2	24.86	23.58	23.34	23.06	0.97	42882	Q	2.726	BLAGN	260	4.88e-15
116	03:33:39.78	-27:56:47.6	23.67	0.220	4.1	J033339.81-275647.7	23.92	23.21	22.98	22.04	0.01						
117	03:32:02.43	-28:10:47.3	23.75	0.205	3.3	—											
118	03:32:21.01	-27:40:29.4	23.76	0.314	7.3	J033221.02-274030.0	23.69	23.48	23.62	23.04	0.31	49352	G				<5.71e-16 ^e
119	03:33:40.03	-28:09:08.3	23.83	0.207	3.2	—											
120	03:33:14.85	-27:57:49.1	23.79	0.204	3.1	J033314.86-275749.3	25.35	23.70	23.96	23.48	0.87	13244	Q			625	1.05e-15
121	03:31:47.90	-27:48:31.0	23.85	0.270	5.6	J033147.91-274831.2	23.88	23.99	23.42	23.07	0.07	32231	G	0.652	em		<5.13e-16 ^e
122	03:31:59.51	-27:50:21.7	23.89	0.224	3.8	J033159.53-275021.6	23.90	23.82	23.66	23.53	0.23	28406	G				<5.71e-16 ^e
123	03:31:51.01	-27:39:33.4	23.89	0.219	3.6	J033151.04-273933.6	23.99	23.71	23.65	23.38	0.10	51258	G				
124	03:32:21.64	-27:39:21.5	23.90	0.266	5.2	J033221.64-273921.9	24.41	23.16	22.77	22.16	0.22	51796	G				<5.49e-16 ^e
125	03:31:47.94	-27:50:45.5	23.91	0.292	6.0	J033147.98-275045.5	23.85	23.51	23.78	23.61	0.56	27530	G	1.065	BLAGN	170	<1.56e-15
126	03:32:35.37	-27:49:20.6	23.92	0.261	4.5	J033235.38-274920.8	23.97	23.81	23.78	23.51	0.15	30561	G	0.666	g		<6.00e-16 ^e
127	03:32:42.00	-27:50:51.9	23.93	0.233	3.6	J033242.02-275052.0	25.06	23.97	24.06	23.63	0.13	27422	G				<5.44e-16 ^e
128	03:31:34.18	-27:38:46.1	23.93	0.296	3.8	J033134.16-273846.2	23.62					52868	G				
129	03:33:39.09	-27:52:56.1	23.93	0.307	3.8	J033339.09-275256.4	24.19	23.79	22.58	22.87	0.13						
130	03:32:28.65	-27:38:46.5	23.95	0.250	4.0	J033228.65-273846.8	24.32	24.31	24.02	23.57	0.10	52921	G				<9.66e-16 ^e
131	03:32:35.36	-28:00:41.2	24.00	0.357	5.7	J033235.38-280041.4	24.58	24.45	24.07	23.76	0.02	7139	Q/G			408	2.22e-15
132	03:33:31.11	-27:59:28.7	24.02	0.246	3.8	J033331.13-275929.0	23.96	23.97	23.72	23.79	0.20	9765	G				

^a COMBO-class: G=galaxy, Q=QSO, S=star, U=unclear (Wolf et al. 2004)

^b BLAGN=Broad Line AGN, LEX=Low Excitation spectrum, NELG=Narrow Emission Line Galaxy (Szokoly et al. 2004); q=quasar, em=emission line galaxy (Ravikumar et al. 2007); g=galaxy (Grazian et al. 2006); SN=supernova, SNC=supernova candidate (Botticella et al. 2008); EN=extranuclear (Hornschemeier et al. 2004; Lehmer et al. 2006)

^c From Lehmer et al. (2005) unless otherwise noted

^d From Giacconi et al. (2002)

^e Our estimate